Hindawi Publishing Corporation
Advances in High Energy Physics
Volume 2014, Article ID 250646, 8 pages
http://dx.doi.org/10.1155/2014/250646

Research Article

Performance of Water-Based Liquid Scintillator: An Independent Analysis

D. Beznosko, A. Batyrkhanov, A. Duspayev, A. Iakovlev, and M. Yessenov

Department of Physics, Nazarbayev University, Astana 010000, Kazakhstan

Correspondence should be addressed to D. Beznosko; dima@hitecht.us

Received 5 April 2014; Accepted 14 July 2014

Academic Editor: Abhijit Samanta

The water-based liquid scintillator (WbLS) is a new material currently under development. It is based on the idea of dissolving the organic scintillator in water using special surfactants. This material strives to achieve the novel detection techniques by combining the Cerenkov rings and scintillation light, as well as the total cost reduction compared to pure liquid scintillator (LS). The independent light yield measurement analysis for the light yield measurements using three different proton beam energies (210 MeV, 475 MeV, and 2000 MeV) for water, two different WbLS formulations (0.4% and 0.99%), and pure LS conducted at Brookhaven National Laboratory, USA, is presented. The results show that a goal of ~100 optical photons/MeV, indicated by the simulation to be an optimal light yield for observing both the Cerenkov ring and the scintillation light from the proton decay in a large water detector, has been achieved.

1. Motivation

In large water detectors, the Cerenkov radiation produced by a charged particle above the threshold can be used for particle identification and the reconstruction of its direction and energy [1]. However, all charged particles below the Cerenkov threshold are missed. Detecting these below-threshold particles is important for various applications, for example, in the search of the proton decay, in the $p^+ \rightarrow K^+\overline{\nu}$ channel, where K^+ is mostly below Cerenkov threshold and is invisible in a water detector. The use of the WbLS makes the kaon visible and allows for the separation of K^+, μ^+, and e^+ signals using timing and thus reducing the background for this decay channel. The same goes for the quasielastic collisions in the large water-based neutrino detectors such as Super Kamiokande detector [1] with proton often being below the Cerenkov threshold and thus not visible.

In either LS or WbLS, the isotropic scintillation light is produced by the charged particle energy deposition via ionization, but the scintillator components may interfere with the Cerenkov ring detection. To detect K^+ and preserve the Cerenkov ring, MC studies indicate that the light yield (LY) from the scintillator component in the WbLS should be 100 optical photons/MeV [2].

Thus, WbLS potentially combines both the Cerenkov ring and scintillation light capabilities. It can preserve the particle identification for the particles above the Cerenkov threshold and detect the charged particles below the threshold via the scintillation light. In addition, WbLS features the lower cost than pure LS and it is safer to handle [3].

The ability to reach the desired LY can be checked using the monoenergetic proton beam with different WbLS concentrations. For the test, the two different WbLS formulations (0.4% and 0.99%), pure water and pure LS samples, were chosen. Three different proton beam energies were used with each sample. The choice of the energies comes from the following considerations:

(i) 2000 MeV protons behave as minimum ionizing particle (MIP);

(ii) 475 MeV protons are just below the Cerenkov limit in water;

(iii) 210 MeV protons have ~same energy deposition as K^+ from the proton decay channel mentioned above.

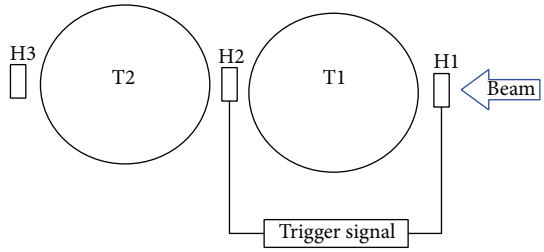

Figure 1: Proton beam test experimental setup.

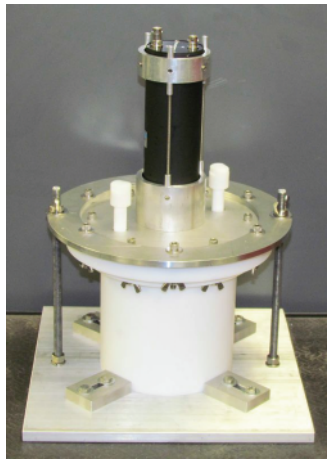

Figure 2: PTFE tub detector with a PMT.

2. Experimental Setup

The experimental setup used for the proton beam test is shown in Figure 1. Two tubs with the samples were used (T1 and T2). Three 2 cm × 2 cm and 5 mm thick plastic scintillator hodoscopes were used (H1 to H3) with the beam trigger being formed by the coincidence of the H1 and H2 only. H3 was intended to verify whether particles exit T2.

2.1. Tub and Signal Readout Description. Two tubs were used in the experiment:

(i) T1 from polytetrafluoroethylene (PTFE) (white, highly reflective),

(ii) T2 from aluminum, coated with black PTFE (very low reflectivity).

The T1 allows the capture of most of the light produced in the tub (~75% of the total light produces in the tub), whereas T2 allows for the observation of the light coming directly from the scintillation without the multiple wall reflections (~10%) as it was coated with black material on the inside. An image of a tub is in Figure 2. Both T1 and T2 have the same dimensions:

(i) lid is 19.05 mm thick;

(ii) walls and bottom are 6.35 mm thick;

(iii) inner height and diameter are 150 mm.

A detailed setup readout scheme is shown in Figure 3. Both tubs (and hodoscopes) were read out by Hamamatsu Photonics [4] R7723 $2''$ Photomultiplier tubes (PMT). A transparent to the ultraviolet light acrylic window was used as a partition between the PMT and the liquid in the tub. The window was protruding through the lid and into the liquid by several millimeters to ensure that there are no air bubbles on its surface.

A readout was performed by the 4-channel 14-bit CAEN [5] V1729A flash analog-to-digital converter (FADC). All tubs signals were connected to the FADC via a variable attenuation unit (Phillips Scientific [6] 804) and a variable amplifier unit (Phillips Scientific 778) with two equal outputs. For the T1 and the T2 readouts, the gain was set to the value of ~2x. The first output from the amplifier goes to the FADC, with a dedicated channel for each tub. The second output from each amplifier channel was used for the single photoelectron (PE) calibration. The gain for the second amplification stage was set at ~10x.

All hodoscopes were also connected via ~2x gain amplifiers that allowed output signal splitting into two. H1 and H3 share the same FADC channel with the latter signal being delayed by 200 ns. H2 was connected to the last remaining channel of the FADC.

2.2. Triggering Scheme. Triggering schema was realized using three 2 cm × 2 cm, 5 mm thick plastic scintillator counters that were readout by $2''$ PMTs via an air waveguide in order to remove the PMTs from direct beam exposure. The signals from the front-most and the middle counters (H1 and H2) were used to form a beam trigger, as indicated in Figure 3.

2.3. Proton Beamline Description. A proton test beam was conducted at NASA Space Radiation Laboratory (NSRL) facility at BNL [7]. As described above, the three following proton beam energies were used: 210 MeV, 475 MeV, and 2 GeV. The beam had the following main characteristics:

(i) intensity was ~1p^+/bunch;

(ii) beam size was 1 cm × 1 cm at 2 GeV and 5.4 cm × 5.4 cm at 210 MeV;

(iii) 0.4 s long spills every ~4 sec.

3. Data Analysis

3.1. Liquids Measured. A surfactant (linear alkylbenzene sulfonic acid, LAS) is used to dissolve the 1,2,4-trimethylbenzene, or pseudocumene (PC), which is a common LS material, in water. The PPO (2,5-diphenyloxazole) and MSB (1,4-Bis(2-methylstyryl) benzene) are used as a fluor and a wavelength shifter to downshift the ultraviolet light from the LS to the blue region of the spectrum where water has higher transparency. Further details can be found in [3].

The composition of the 4 samples tested in this experiment are as follows:

(i) water (purified);

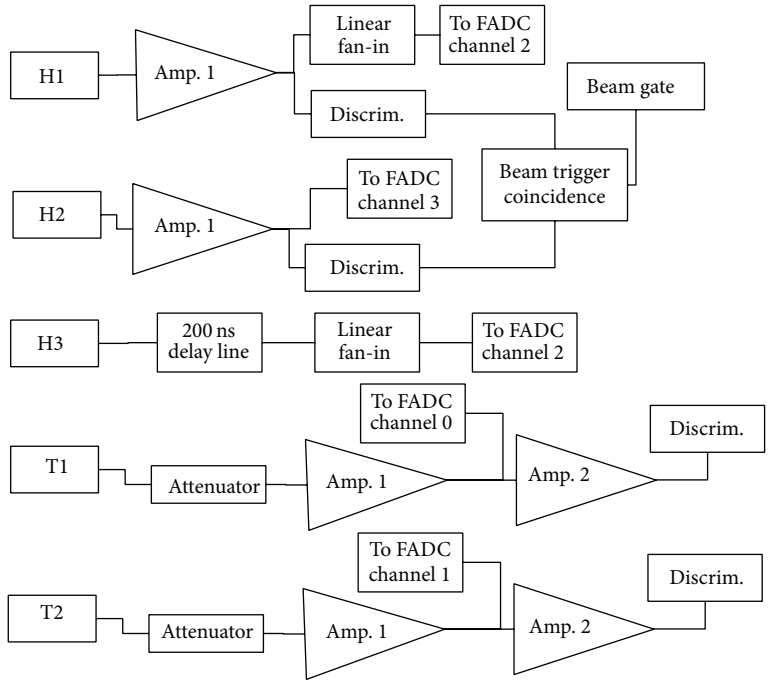

Figure 3: Proton beam test electronics readout setup.

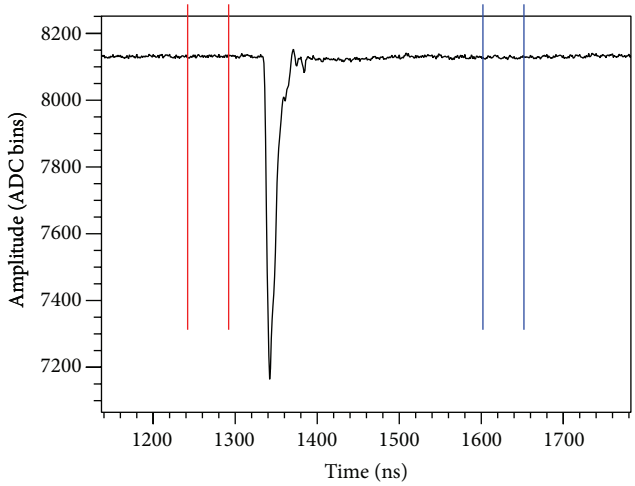

Figure 4: Typical PMT waveform with baseline check windows.

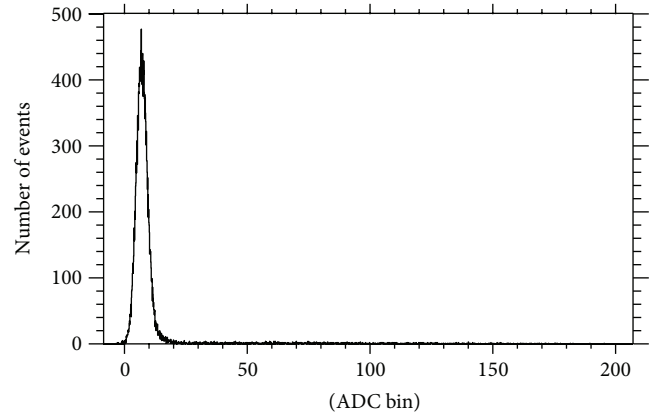

Figure 5: Typical baseline value for a single channel.

(ii) WbLS1: 0.4%PC + 0.4 g/L PPO + 3 mg/L MSB + surfactant in water;

(iii) WbLS2: 0.99%PC + 1.36 g/L PPO + 7.48 mg/L MSB + surfactant in water;

(iv) LS: LAB + 2 g/L PPO + 15 mg/L MSB.

3.2. Waveform Analysis. The PMT signal is acquired as a waveform with a sample shown in Figure 4. Total acquisition window is 2560 bins per event with each bin being 1 ns wide; the approximate position of the signal is known beforehand. A 300 ns window (central one in the figure, between the red and blue lines) is used to obtain the integrated signal area by summation. Each point is subtracted from the average baseline to achieve a positive sum. A typical signal is smaller than the chosen window width; however, there is a small spread in the timing of the signals and we want to be sure that signal's entire area has been integrated. The size of the chosen window is the same for all samples and measurements.

A baseline is defined as the average value of all the points in the first integration window (between the two red lines) that is 50 ns wide. A typical baseline is shown in Figure 5. To check the baseline quality, its averaged value is compared with the average of the postsignal window (between the two blue lines). This difference is illustrated in Figure 6. Events with this difference larger than ~20 ADC bins are flagged as bad. This allows for the removal of the noise events or events with the bad baseline due to the shifted signal or multiparticle

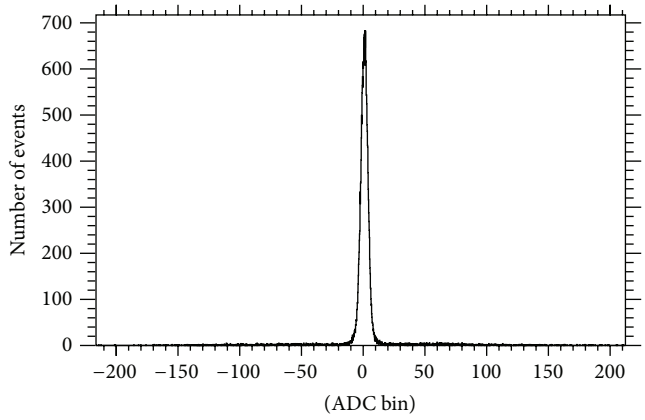

Figure 6: Difference between the baseline and the average of the postsignal window.

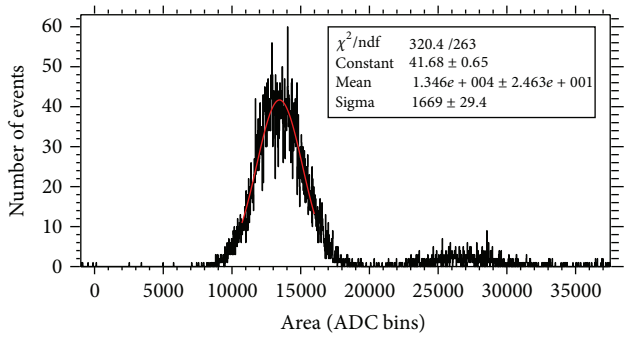

Figure 7: A sample fit of a tub signal.

events. Additionally, a comparison of the baseline with an average of a window at the very beginning of the waveform (between 10 ns and 40 ns, not shown because the figure is zoomed around the signal area) is used for general baseline quality check using the above criterion.

The integrated area is a measure of total charge that can be converted to the PE yield using the single PE calibration of the PMTs. This allows the description of the measured signals independent of the hardware differences between the channels.

The trigger information is saved with the data. This allows the offline trigger requirements to be used later during the analysis stage.

3.3. Single Photoelectron Calibration. A single PE calibration was conducted for both T1 and T2 signal channels at the end of the test beam run. The trigger for this calibration is produced by the discriminator that is connected to the second amplifier for the T1 and T2 signals (separately, for each channel, see Figure 3). The discriminator is set to ~ 1/10th of the single PE amplitude so as to allow for better PE signal detection efficiency than using purely random trigger. Additionally, this forces the PE signal into the signal window region of the FADC output for the simplified analysis and elimination of the partially captured signals. Note that a PE signal is much narrower and lower in amplitude/area

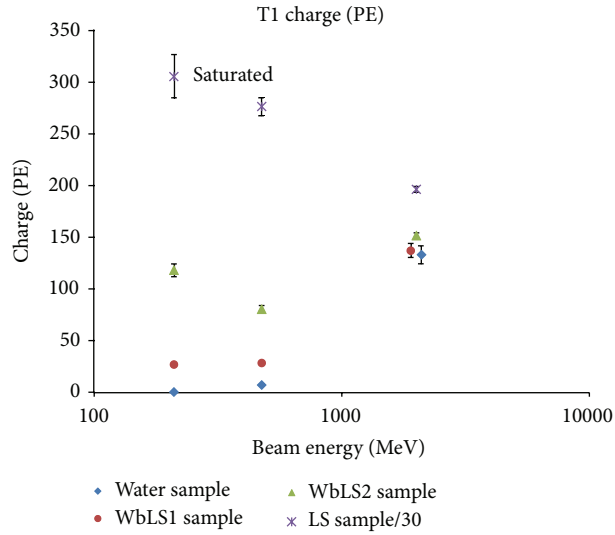

Figure 8: The light yield in PE for T1. At 2 GeV beam energy, some points are offset for clarity.

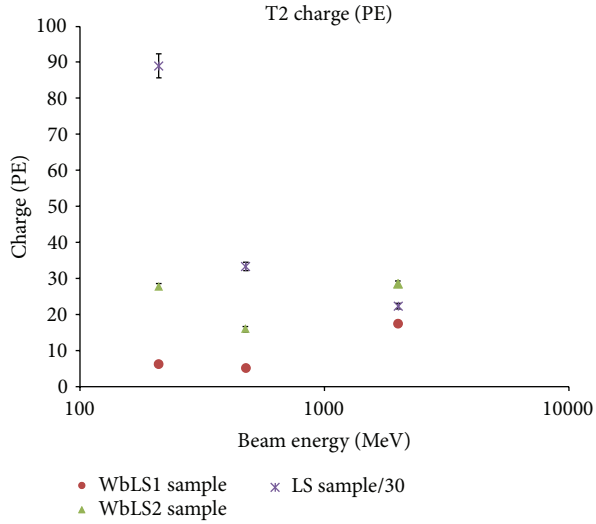

Figure 9: The light yield in PE for T2.

than the beam signals as they are typically many PEs that arrive according to some time distribution; thus a smaller integration window is used to reduce noise for cleaner calibration (50 ns instead of 300 ns).

The calibration signal area is 168.0 ± 1.2 ADC bins and 132.9 ± 1.6 ADC bins for T1 and T2, respectively (the PE signal is summed within the window, so the unit of ADC bin is still used). A special care was taken to verify that this method yields the same calibration values as using the light-emitting diode (LED) scheme. For that, calibration runs using the scheme described above and using the dim LED pulses were compared to each other. The LED light level is chosen such that only ~1/10th of the events has the single PE signal to ensure that these are indeed the single photon detection responses.

Table 1: Energy deposition in samples.

Beam energy (MeV)	Sample	T1 energy deposit (MeV)	T2 energy deposit (MeV)
210	Water, WbLS	72.7 ± 3.1	107.5 ± 6.1
	LS	59.2 ± 2.5	124.1 ± 7.0
475	Water, WbLS	40.4 ± 2.0	43.7 ± 2.2
	LS	34.4 ± 1.7	36.3 ± 1.9
2000	Water, WbLS	28.6 ± 2.6	28.7 ± 3.1
	LS	24.1 ± 2.3	24.2 ± 2.7

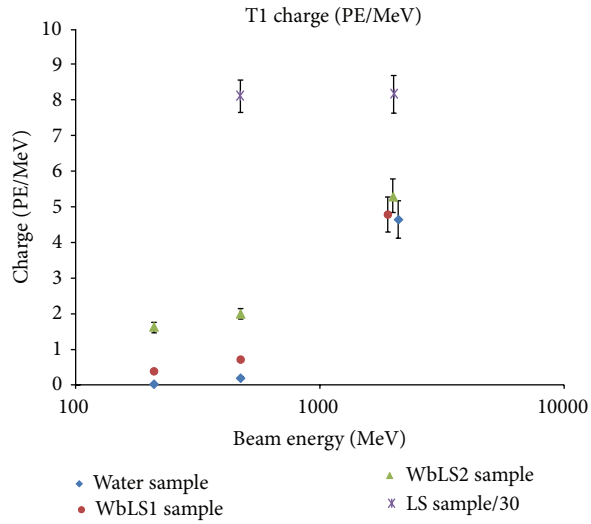

Figure 10: The light yield in PE/MeV for T1. At 2 GeV beam energy, some points are offset for clarity.

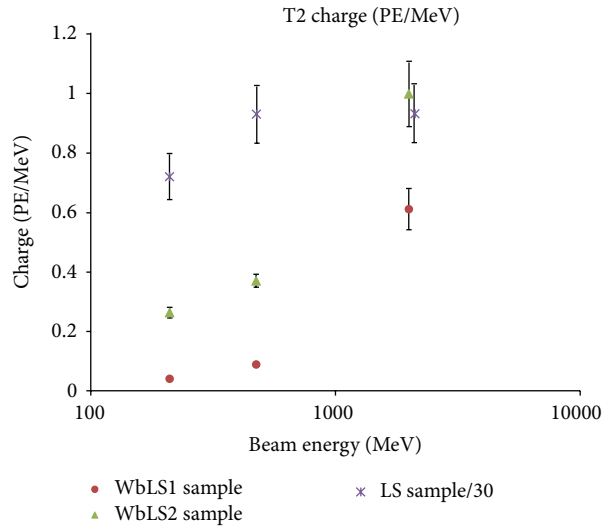

Figure 11: The light yield in PE/MeV for T2. At 2 GeV beam energy, some points are offset for clarity.

3.4. Data Quality Selection. The data quality check is done as a single step before the data is analyzed. The care was taken to choose the criteria that do not introduce a bias into the selection. These are

(i) offline double trigger requirement for H1 and H2 to be above ~50 mV and within the expected time window;

(ii) baseline quality check as outlined in Section 3.2;

(iii) ADC saturation check for H1 and H2.

Each check is intended to remove potential noise or multiple particles in an event. The saturation check indicates that several particles have passed through the hodoscopes in a same beam spill, which happens very rarely at the beam intensity used.

3.5. Light Yield Results. For each sample and energy, a histogram of the signal areas is computed. A Gaussian fit using a bin likelihood method is then performed. The fitting is done in two steps. First, a Gaussian is fitted in the range between the half of the maximum peak values to obtain the first approximation for the peak position. Then, the fits around the found mean with 1, 1.5, and 2σ are carried. This is done to estimate the uncertainty that the fitted signal width

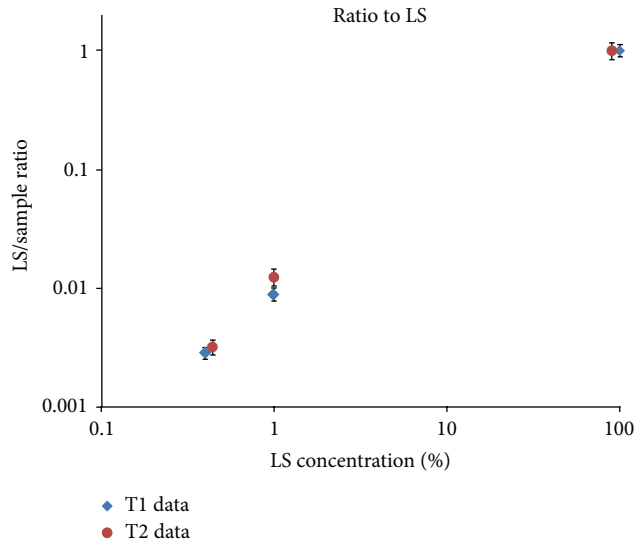

Figure 12: The WbLS light yield ratio to LS at 475 MeV. Some points are offset for clarity.

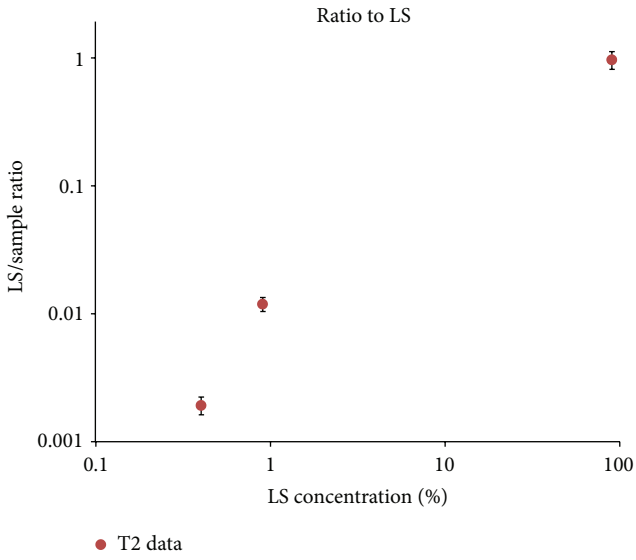

Figure 13: The WbLS light yield ratio to LS at 210 MeV. Only data for T2 is shown.

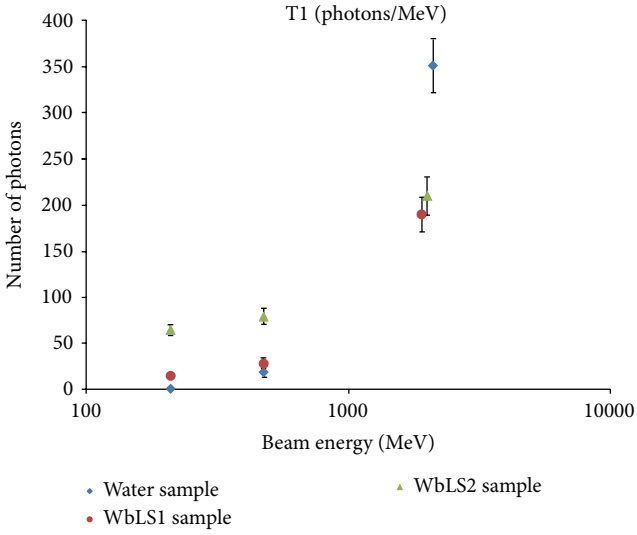

Figure 14: The light yield in photons/MeV for T1. At 2 GeV beam energy; some points are offset for clarity.

limitation is added to the mean. This is because there is the second peak to the right of the main one, from the second particle, rarely passing through the tub during the same trigger time. Figure 7 shows the 1.5σ fit of the first particle peak, and the second particle peak is visible on it as well. This plot is in the ADC bins for clarity; single PE calibration will be applied to all further plots.

The data for all the samples and all energies is then processed in the same way. Plots in Figures 8 and 9 show that the light yield results in PE for the different samples and beam energies for T1 and T2, respectively. Note that the light yield values for LS are reduced by a factor of 30 on these plots. In addition, the data point for the LS at 210 MeV for T1 is not going to be shown on further plots because of the readout

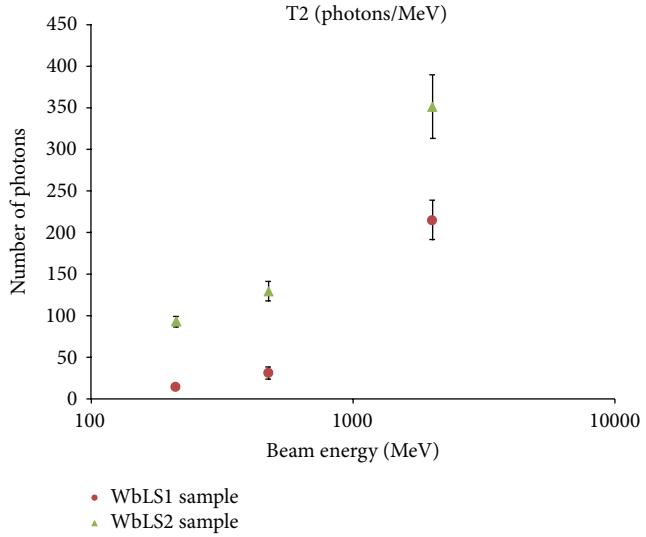

Figure 15: The light yield in photons/MeV for T2.

saturation due to the large light yield from the scintillator at this energy. Similarly, the water data is not shown for T2 due to the very low signal for proton energies below the Cerenkov limit.

3.6. Energy Deposition. In order to assess the PE/MeV light yield of each sample, the energy deposition in each sample is needed. Two methods were used for this purpose. The first one uses a GEANT4 simulation of the proton beam with the most likely deposition being the mean of the 1000 runs at each energy. Second one is a simplified code [8] that would calculate the proton energy loss along a straight line path through the tubs and hodoscopes with small steps, using the proton stopping power and range (PSTAR) tables from the National Institute of Standards and Technology (NIST). The WbLS was modeled as water and LS as toluene.

The resulting energy depositions are listed in Table 1. The values are taken from the GEANT4 simulation results, and the difference between two methods is taken as the uncertainty for the values obtained. The light yield from the data that is converted into the PE/MeV is shown in Figure 10 for the T1 and in Figure 11 for the T2.

We see that the PE/MeV light yield is the same for LS at proton energies of 2 GeV and 475 MeV on both tubs, indicating that the Cerenkov light contribution is negligible for LS. It is not the same for the WbLS as there is a significant LY change between these two energies. However, at 475 MeV, there is virtually no Cerenkov light contribution to the total LY (as indicated by the very small amount of light at this energy in water in T1). Thus, we can use the data at this energy for LS to WbLS comparison and for obtaining the LY of the scintillator components of the WbLS. From the data, Figures 12 and 13 show the ratio of the WfbLS signal to the LS signal for the T1 and T2 at the proton energy of 475 MeV, and the same ratio for the T2 only for the 210 MeV (due to the saturation of the LS signal in T1 at this energy, it is not used in the analysis).

3.7. Light Yield in Photons/MeV. An estimate of the LY in photons/MeV is also possible. The calibration is needed here to estimate the efficiency of the PMT readouts from the T1 and T2. Typically, this is a difficult task to carry out precisely, so two simple methods have been used to do this estimate.

The first method is based on the fact that the LY in photons for the LS is known to be 10 k photons/MeV for a MIP signal [9]. Since the proton at 2 GeV has the ~same dE/dx as MIP, this LY value can be used to get the approximate efficiency for each tub (e.g., PE to photon conversion) for the WbLS data. The second one can be used for T1 only to check the validity of the first method. The difference between the methods was added to the total uncertainty of the result.

As mentioned above, a second method for the efficiency check was done for T1. We can use the 2 GeV proton data on water to get the readout efficiency; first we need to try and estimate the number of the protons produced in water using (1) that is commonly used to estimate the photon LY for the Cerenkov radiation in water as follows:

$$\frac{dN}{dx} \approx 370z^2 \left(E_{\max} - E_{\min} - \frac{1}{\beta^2} \frac{E_{\max} - E_{\min}}{n_{\text{ave}}^2} \right). \quad (1)$$

The average index of refraction for the optical range was used, and the $E_{\max}$ and $E_{\min}$ have been taken from the PMT sensitivity data. To get a better estimate, the sensitivity range for the T1 PMT was divided into a number of small subranges with ~constant sensitivity. The results for each subrange were weighted by the sensitivity at that range and combined together for a better estimate. Then, an efficiency calibration is obtained.

Using the resulting calibration of PE to photon conversion, now the 2 GeV proton LS data was used to compare the number of PE produced by the second method to the value taken as a base in the first method (which was 10000 photons/MeV). The result came very close to be 9713 photons/MeV for the LS using the efficiency from the Cerenkov light for T1.

The final estimate results for the WbLS data are presented in Figures 14 and 15 for the T1 and T2, respectively. As it can be seen from these figures, the estimate shows that the goal of about 100 photons/MeV has been reached using the WbLS2 sample, and different LY are possible by adjusting the concentrations.

3.8. Systematics. A number of the systematic effects have been identified. Their effects have been accounted for in all the results presented.

During the experiment, the tubs with samples had to be disconnected and samples changed. An effect on the PMT of turning biasing on and off and exposing the PMT to ambient light during the disconnects was tested. There is some minor variation in PMT noise and gain for less than 2 minutes after bias is turned on before a steady state is reached. Typically, there was at least a 5- to 10-minute interval between installing the new sample in the beamline and data taking (the time was needed for the beam tuning process), thus greatly diminishing the influence of this effect on the data. In addition, a very small variation in gain between each steady state was noted; this variation has been added into the single PE calibration uncertainty.

A long-term stability of the single PE calibration was studied separately using the data taking run that was 450 hours. The LED calibration was collected during the entire run in 2 h periods and the resulting calibration variation (~1%) was added into the single PE calibration uncertainty.

The effects on the result due to the fitting procedure have been described in Section 3.5.

Another systematic effect arises from the window size selection process during the waveform analysis described in Section 3.2. The integration window size had to be optimized to fit all signal widths from all the data samples collected. If the window is too narrow then some signal may be lost in the integration, and if it is too large, too much noise will be integrated together with the signal and may add a nonzero contribution due to some of the noise not being random. A comprehensive study was carried out to determine the window size (300 ns) and the effect of this choice on the fitted means for each sample. The effect turned out to be small (the largest contribution of this effect is being less than ~0.5% for one of the samples, while it is being even smaller for all others) and it is accounted for in the total fit uncertainty together with the uncertainties estimated due to the fitting procedure.

4. Conclusion

The LY for the water, pure LS, and two formulations of the WbLS have been measured successfully. The 0.99% WbLS sample yields ~1% light of the pure LS, implying that the goal of 100 photons/MeV has been achieved and assuming that typical LY of LS is 10000 optical photons per MeV. Therefore, the WbLS that satisfies the requirements for the K^+, μ^+, and e^+ detection can be fabricated. The result also illustrates that different LY can be easily achieved by adjusting the WbLS components concentration.

The next experiment that will allow for the separation of the Cerenkov and scintillation light in WbLS has been conducted and the data is being analyzed. In addition, the work is planned at Nazarbayev University to carry out the optimization of the composition of the WbLS formulation.

Conflict of Interests

The authors declare that there is no conflict of interests regarding the publication of this paper.

Acknowledgments

The authors thank the Electronic Detector Group at BNL for the opportunity to work with them at this experiment. Also they thank the Chemistry Group of Dr. M. Yeh at BNL Chemistry Department.

References

[1] M. Fechner, K. Abe, Y. Hayato et al., "'Kinematic reconstruction of atmospheric neutrino events in a large water Cherenkov

detector with proton identification," *Physical Review D*, vol. 79, Article ID 112010, 2009.

[2] C. Zhang, "A large water-based liquid scintillation detector in search for proton decay $p \rightarrow K^{+}\overline{\nu}$ and Other Physics," in *Proceedings of the American Physical Society Meeting*, abstract #L12.005, April 2013.

[3] M. Yeh, S. Hans, W. Beriguete et al., "A new water-based liquid scintillator and potential applications," *Nuclear Instruments and Methods in Physics Research A*, vol. 660, pp. 51–56, 2011.

[4] Hamamatsu Photonics, Shizuoka, Japan, http://www.hamamatsu.com.

[5] CAEN (Costruzioni Apparecch iature Elettroniche Nucleari S.p.A.), Via della Vetraia 11, 55049 Viareggio, Province of Lucca, Italy, 0584 388398.

[6] Phillips Scientific, "31 Industrial Ave. Suite 1," Mahwah, NJ, USA.

[7] Brookhaven National Lab, PO Box 5000, Upton, NY 11973-5000.

[8] D. Jaffe, "Preliminary results on water-based liquid scintillator in a proton beam," in *2nd Open Meeting for Hyper-Kamiokande Project*, January 2013.

[9] C. Aberle, A. Elagin, H. J. Frisch, M. Wetstein, and L. Winslow, "Measuring directionality in double-beta decay and neutrino interactions with kiloton-scale scintillation detectors," *Journal of Instrumentation*, vol. 9, 2014.